EL NIÑO MEETS LA NIÑA – ANOMALOUS RAINFALL PATTERNS IN THE "TRADITIONAL" EL NIÑO REGION OF SOUTHERN ECUADOR

Jörg Bendix, Katja Trachte, Enrique Palacios, Rütger Rollenbeck, Dietrich Göttlicher, Thomas Nauss and Astrid Bendix

With 8 figures, 1 table and 1 photo
Received 17. October 2010 · Accepted 17. March 2011

Summary: In this paper, the central Pacific cold event of 2008 and its exceptionally warm conditions in the eastern tropical Pacific are analyzed by using rainfall data of south Ecuadorian meteorological stations, sea surface temperatures in the El Niño3 and 1+2 regions, and simulations with the Weather Research and Forecasting (WRF) model. It can be shown that El Niño-like rainfall conditions with severe inundations occur particularly in the coastal plains of southern Ecuador while a central Pacific cold event prevails. In contrary to previous situations, positive rainfall anomalies as a result of El Niño-like conditions in the El Niño1+2 region during the 2008 La Niña event occurred in both regions, the coastal plains and the highlands, for the first time. A detailed analysis of the ocean-atmosphere system during episodes of heavy rainfall reveals typical El Niño circulation and rainfall patterns as observed during previous El Niño events for the coastal area and La Niña-like conditions for the highlands. The spreading of Pacific instability in the Niño1+2 region to the eastern escarpment of the Andes could be the result of a temporary eastward shift of the Walker circulation. The unusual combination of El Niño-like conditions in the eastern tropical Pacific during a La Niña state in the central Pacific is the newest indicator for an impact mode shift regarding severe rainfall anomalies during El Niño/La Niña events in the traditional El Niño area of southern Ecuador since the end of the last century. Since 2000, El Niño events unexpectedly provide below average rainfall while central Pacific La Niña conditions generate exceptional severe flooding in the normally drier coastal plains. The novel sea surface temperature (SST) anomaly dipole structure between the eastern and central/western tropical Pacific and the weakening of El Niño events since 2000 could be due to natural decadal oscillations in the El Niño background state, the Pacific Decadal Oscillation (PDO). However, the observed atmospheric patterns and the recent increase of the SST anomaly difference between the central and the eastern tropical Pacific resemble structures that also result from climate change simulations.

Zusammenfassung: Mit Hilfe von meteorologischen Messdaten, Meeresoberflächentemperaturen des tropischen Pazifiks und Simulationen mit dem WRF (Weather Research and Forecasting) Mesoskalamodell wird das mit anormal warmen, küstennahen Meerestemperaturen einhergehende La Niña-Ereignis 2008 für das südliche Ecuador untersucht. Es zeigt sich, dass erstmalig aufgrund El Niño-artiger Bedingungen in der Niño1+2 Region hohe Niederschläge insbesondere im Küstenvorland Ecuadors zeitgleich zu einem offiziell verlautbarten La Niña-Ereignis im Zentralpazifik auftreten. Gleichzeitig sind auch im Hochland hohe Niederschläge zu verzeichnen, die normalerweise nur in einem La Niña-Jahr (mit trockener Küstenebene) auftreten. Diese neuartigen Wetterverhältnisse könnten mit einer Ostwärtsverlagerung der zonalen Walker-Zirkulation verknüpft sein. Insgesamt ist das 2008-Ereignis ein weiteres Indiz für eine Veränderung des ENSO-Systems und seines Einflusses auf die ENSO-Kernregionen Ecuador und Nordperu. Es zeigt sich, dass seit 2000 El Niño-Ereignisse weniger intensiv ablaufen, während im Zuge von La Niña-Events unüblich hohe Niederschläge in dem normalerweise deutlich zu trockenen Küstenvorland auftreten. Die dafür verantwortliche, neuartige Dipolstuktur der Meeresoberflächentemperaturen im tropischen Pazifik (Kalte La Niña-Bedingungen in der 3+4 Region, warme El Niño-Bedingungen in der 1+2 Region) könnte eine Folge der Pazifischen Dekadischen Oszillation (PDO) sein, die zum Jahrtausendwechsel von der Warm- in die Kaltphase gewechselt ist. Ähnliche Zirkulationsmuster ergeben allerdings auch jüngste Klimawandel-Szenariorechungen, sodass beim derzeitigen Forschungsstand nicht entschieden werden kann, ob die beschriebenen Anomalien im ENSO-Kerngebiet in Ecuador und Nordperu natürlichen oder anthropogenen Ursprungs sind.

Keywords: El Niño, La Niña, ENSO, South Ecuador, rainfall anomalies, sea surface temperature anomalies

1 Introduction

The El Niño/La Niña (EN/LN) phenomenon is one of the most investigated natural atmospheric systems. It is generally related to warm/cold pool oscillations in the tropical Pacific and the tropical Walker circulation, summarized in the ENSO concept (El Niño-Southern Oscillation) (Wyrtki 1975; Zebiak and Cane 1987 and many others thereafter). The classification of EN and LN events is frequently con-

DOI: 10.3112/erdkunde.2011.02.04 ISSN 0014-0015 http://www.erdkunde.uni-bonn.de

ducted by means of the classical Southern Oscillation Index (SOI), which should be <-1 (>1) for a warm (cold) event (e.g., Kiladis and van Loon 1988). Many other indices had been evolved under different foci to characterize the Pacific EN/LN status. For example, the American Weather Service frequently uses the N3 or N3.4 Index regarding the sea surface temperatures (SST) in the N3 resp. N3.4 region, the Oceanic Niño Index (Smith and Reynolds 2003 and 2004), the Multivariate ENSO Index (Wolter and Timlin 1998) and the Trans-Niño Index by Trenberth and Stepaniak (2001). Several theories like the Delayed-Oscillator-Theory have been developed over the last decades to describe a typical ENSO regime (Zebiak and Cane 1987; Suarez and Schopf 1988;), but all past events exhibited slightly different behaviours (for the "traditional" EN area of Ecuador refer for instance to Bendix 2000a; Bendix et al. 2003; Takahashi 2004; Douglas et al. 2009). More recently, atmospheric patterns like the Madden-Julian-Oscillation (e.g., Takayabu et al. 1999; Kessler 2001) and Westerly Wind Bursts (WBB) (e.g., Waliser et al. 2003) have interacted with ENSO, particularly being responsible for the onset as well as the specific characteristics of single events. Because EN/LN can cause devasting droughts and floods especially in the Maritime Continent and South America (Glantz 1984; Ropelewski and Halpert 1987), a proper ENSO forecast as well as a prognosis of global climate change effects on ENSO intensity and impacts is needed. While in the 80s of the last century, ENSO forecasts seemed on the way to becoming possible (e.g., Barnett et al. 1988), in the following years, the complexity of the phenomenon made short-term forecasts as well as long-term prognoses with numerical models a difficult and to date not satisfactorily accomplished task (Kerr 1999; An et al. 2005; Latif and Keenlyside 2009).

From a statistical point of view, the increase (decrease) of EN (LN) in the last century since 1970 was claimed to be most unlikely due to natural variability (Trenberth and Hoar 1997). However, apparent changes in EN/LN are supposed to be the result of decadal variations in the background state of ENSO (An et al. 2005), which might be altered by global warming likewise (Fedorov and Philander 2000). One important element of the ENSO background state seems to be the Pacific Decadal Oscillation (PDO), a 20-30 year fluctuation pattern of the Pacific Ocean (Pavia et al. 2006; Schoennagel et al. 2006). With regard to global warming, the Walker circulation in the tropical Pacific is assumed to be weakening (Power and Smith 2007; Vecchi and Soden 2007) and consequently, EN should decrease to lower amplitude events in a warmer future (Meehl et al. 2006). Due to the poor representation of the ENSO phenomenon in numerical models, several studies underline the great importance of monitoring the change of EN/LN with observational data (Latif and Keenlyside 2009; Vecchi 2008). One of the most sensitive regions to observe changing meteorological impacts of EN/LN events is the "traditional" Niño region in southern Ecuador (e.g., McPhaden 2004; Takahashi 2004) on the east coast of tropical South America. Severe flooding (droughts) normally occur during January and April of an EN (LN) year, particularly in the coastal plains (Bendix and Bendix 1998; Bendix 2000b; Bendix et al. 2003; Vuille et al. 2000 and 2003), while the highlands and the eastern escarpment of the Andes react with anomalously dry (wet) conditions (Vuille et al. 2003; Bendix and Bendix 2006).

At the end of 2007, a new Pacific LN event emerged, peaking in February 2008. Unexpectedly, this event was accompanied by El Niño-like flooding in the coastal plains of the "traditional" El Niño area (southern Ecuador and the north Peruvian Sechura desert; see Photo 1). Affected provinces in the coastal plain of Ecuador were El Oro, Esmeraldas, Guayas, Los Ríos, and Manabí. 63,596 hectares of arable land were completely destroyed by the flooding and some 97,353 hectares were impaired. The inundations affected more than 250,000 people who lacked food, shelter, health, water and sanitation. One result of the exceptional environmental conditions was an increase of water-born diseases like dengue fever in the provinces of Los Rios and El Oro (OCHA 2008 a, b). At the same time, heavy rainfalls un-typically occurred in the highlands of southern Ecuador. In late

Photo 1: Flooding close to Guayaquil (province Guayas) on 10 March 2008 (Photo: J. Bendix)

March 2008, the heavy precipitation led to severe landslides, destroying infrastructure such as e.g., the new connecting road between Catamayo and the provincial capital Loja.

Comparing two mostly reversed El Niño indices for this time, the TNI (Trans-Niño Index) after Trenberth and Stepaniak (2001) and the SOI, the uniqueness of this event is characterized by a clear discordance of both indices for the period January to April 2008: While the SOI shows positive values between 0.56 and 2.05 and therefore indicates strong LN conditions, the TNI values point to strong El Niño conditions by ranging between 2.1 and 2.95. The main goal of the current paper is to analyse the obvious changes in the ENSO regime and to unveil possible causes. A major spatial focus is on a latitudinal transect along the core ENSO area of southern Ecuador, the study site of a multidisciplinary ecological research project where climatic changes might severely affect ecosystem functioning and its services (Bendix and Beck 2009; Fries et al. 2009; Bendix et al. 2010).

2 Study area, data and methods

2.1 Study area

The study area comprises the "traditional" El Niño region of southern Ecuador and the tropical Pacific Ocean, particularly the El Niño3.4 and 1+2 regions (Fig. 1).

The climate of southern Ecuador is clearly affected by the cold Peru Current off the coast of Ecuador in combination with the location of the South Pacific anticyclone. There are pronounced W-E and N-S rainfall gradients at the coast with relatively dry areas south of Guayaquil and towards northern Peru (Sechura desert). Rainfall generally increases towards the higher parts of the west-facing slopes of the Andean cordillera which is characterized by a significant height depression between southern Ecuador and northern Peru (the so-called Huancabamba depression, Beck et al. 2008). The spatial rainfall distribution in the highlands is patchy due the complex terrain structure where pronounced windward and leeward effects cause an alternation between moist (e.g., at Loja) and semiarid conditions (e.g., Catamayo) on a small horizontal distance (e.g., Richter 2003). The eastern escarpment of the Andes reveals per-humid conditions with rainfall between 2000 and >6000 mm (Bendix et al. 2006a; Rollenbeck et al. 2007; Bendix et al. 2008). The annual course of precipitation is characterized by a nearly unimodal peak in March-April in the coastal plains of southern Ecuador, concomitant with the normal El Niño rainfall season. The highlands depict a bimodal regime with two maxima (March-April, October-November) during the equinoxes while the eastern Andean escarpment and the adjacent Amazon area are characterized by rainfall in all seasons, partly peaking in June-July in the higher altitudes (for more details refer to Bendix and Lauer 1992). Besides the general climatic zonation of Ecuador, a detailed analysis of cloudiness by using satellite data reveals that the spatial-temporal structure of rainfall is locally modified by the topographic situation, particularly in the Andean region (Bendix et al. 2004, 2006b).

With regard to sea surface temperature (SST) anomalies, the delineation of El Niño regions in figure 1 follows international standards where the Niño1 region encompasses the cold upwelling area off the coast of northern Peru, the Niño2 region the coastal waters close to the equator and the Niño3 region great portions of the central and eastern equatorial Pacific. The Niño4 region comprises the warm pool of the western Pacific and is thus commonly combined with the Niño3 to the Niño3.4 region (5°N-5°S; 120°-170°W) for the distinction of EN/LN years. For more details, the reader may refer to Cane (1991) and Trenberth and Hoar (1996).

2.2 Data and data analysis

South Ecuadorian rainfall data are available from January 1964 – January 2009 (24 h totals are provided for the period of 19:00 to 19:00 Local Standard Time, hereafter *LST*, LST=UTC-5h) for different locations and provided by the Instituto Nacional de Meteorología e Hidrología del Ecuador (INAMHI).

Anomalies of rainfall for single El Niño/La Niña events are displayed in terms of standard deviation, calculated for the main El Niño/La Niña season (January to April) based on deviations from long-term average and standard deviation:

$$P_{An}^{ev} = (P^{ev} - Av) / \sigma \quad (1)$$

where P_{An}^{ev} is the January-April rainfall anomaly of an event (ev) in terms of standard deviation, P^{ev} the rainfall sum (January to April) of an event (ev) and $Av(\sigma)$ the long term average (standard deviation) of January-April rainfall (1964–2009).

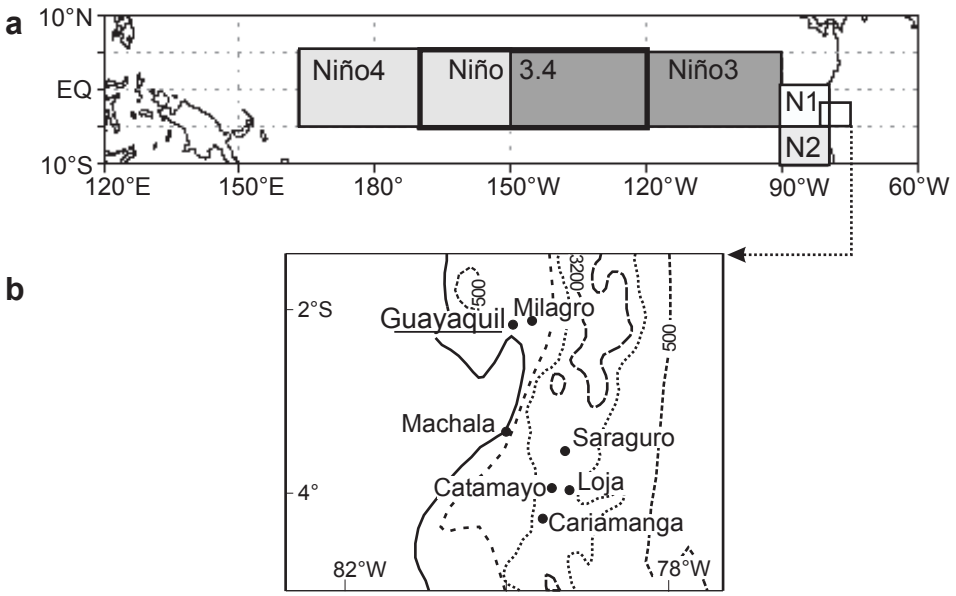

Fig. 1: (a) El Niño regions in the tropical Pacific as internationally used for ENSO research, and (b) location map of meteorological stations in the "traditional" El Niño area used in the current study. Note that isoline labels mark terrain altitude in m a.s.l.

High resolution rainfall data from two stations east of Loja on the eastern Andean slopes (ECSF Estación Científica de San Francisco, lat. 3°58'18" S, long. 79°4'45" W, alt. 1,860 m a.s.l and ECSF-Cerro at 3,180 m a.s.l) are measured in a tropical mountain rainforest with a BIRAL present weather sensor (for more details refer to ROLLENBECK et al. 2007).

Hourly GOES IR satellite data, ingested and processed with the FMet tool at the Marburg satellite station (for more details refer to CERMAK et al. 2008), are inspected visually to analyze the diurnal course and the spatial location of deep convection.

Time series of weekly averaged SST data and anomalies are taken from NOAA's Climate Prediction Center (CPC). The data are generated by means of the Optimum Interpolation (OI) analysis (REYNOLDS and SMITH 1994, 1995). We conducted the SST anomaly difference calculations between the N1+2 and N3.4 regions on the basis of long-term NOAA time series (RAYNER et al. 2003) which are also based on the SMITH and REYNOLDS ERSST.v2 data set. Additionally, data of the Pacific Decadal Oscillation (PDO) index from the National Centers for Environmental Prediction (NCEP) are used, also based on the SMITH and REYNOLDS ERSST.v2 data set. Standard trend and moving average (11 year) analyses are applied to the SST anomaly difference time series and the latter also to the PDO data set. The MODIS (MODerate Resolution Imaging Spectoradiometer) SST product is used, which provides images of average weekly SST. The SST-product is based on the method of WALTON et al. (1998).

2.3 Numerical model

To simulate wind field patterns for the periods of exceptional rainfall of the 2008 event, the mesoscale Weather Research and Forecasting (WRF) model is used. WRF is a fully-compressible and non-hydrostatic model suite with terrain-following vertical coordinates. The equations are solved on an Arakawa C-grid and the time-splitting technique of Runge-Kutta (WICKER and SKAMAROCK 2002).

For the simulations, a two-way-nested domain with 36 km and 12 km is used and 28 sigma levels are selected. The coarse domain has 135 x 51 grid points and is centred at 82.5°W and 3.5°S. The small domain covers an area extending from 85.61 W to 75.17 W and from 1.25°N to 7.23°S, which is large enough to capture N1 and N2 regions. WRF is driven by the NCEP/NCAR reanalysis data, which offers time-dependent lateral boundary conditions (KALNAY et al. 1996) as well. The bottom boundary conditions are provided by the NOAA land-surface model (CHEN and DUDHIA 2001). In order to capture the SST anomaly, we used the 0.5° resolution global NCEP SST data set (GEMMILL et al. 2007).

The model is run with the following set of physics options for both domains: The cumulus convection is parameterized from Kain-Fritsch new Eta model (KAIN and FRITSCH 1993) and the precipitation computations are made by an explicit 3-ice microphysics scheme (LIN et al. 1983). With the Rapid Radiative Transfer Model (RRTM) the longwave (MLAWER et

al. 1997) and shortwave radiation (Dudhia 1989) is simulated. The surface is represented by the Yonsei University (YSU) boundary layer scheme (Hong et al. 2006) including the Monin-Obukhov scheme (Monin and Obukhov 1954).

3 Results

3.1 Rainfall anomalies in southern Ecuador during EN/LN events

Figure 2 and table 1 point out that rainfall anomalies during EN and LN events in the traditional El Niño region of southern Ecuador generally reveal coherent tendencies in the coastal plain (meteorological stations Guayaquil, Machala, Milagro), which particularly hold for the main events of the last century. Until the LN 1999, the coastal stations show weak/moderate positive anomalies during weak/moderate EN events (e.g., EN 1973, 1992) and strong reactions mostly with a rainfall surplus of σ >+3 for strong events (EN 1983, 1998). At the same time, LN events are coherently characterized by drier than normal conditions. The situation at the highland stations is less consistent, but a general tendency can be observed as well: Weak/moderate El Niño situations are related to drier than normal conditions in January to April, while LN conditions normally mean positive rainfall anomalies in the highland. However, it is striking that especially the strong EN of 1983 caused clearly positive anomalies in the area of Cariamanga and Loja. Strikingly, the data shows that these usual impacts of EN/LN abruptly change after the major 1998/99 EN/LN events. EN events in the current century generally seem to decrease in intensity and the impact on rainfall in southern Ecuador reverses. The EN 2002/03 reveals drier (instead of expected moister) than normal conditions in the coastal lowlands, a tendency continuing to the very weak warm event of 2005 (rainfall -0.69 σ for Milagro). At the same time, the most recent LN 2008 shows for the first time in the observations exceptional positive rainfall anomalies in both regions, the coast and the highlands, causing severe inundations at the coast and hazardous landslides in the latter at the same time. This situation seems to initiate a general impact mode change towards an El Niño rainfall regime during central Pacific La Niña conditions and vice versa in the Niño tracer region, the coastal lowlands of southern Ecuador. Hence, it is very important to pinpoint the course of the weather in January to March for the exceptional situation of the 2008 central Pacific cold phase.

3.2 Rainfall in southern Ecuador and SST development during the 2008 event

Figure 3 illustrates the development of SSTs in the central and eastern tropical Pacific and the related rainfall situation at a representative coastal (Milagro) and highland (Loja) station in southern Ecuador. It is shown that periods of extraordinary positive rainfall anomalies in the coastal lowlands start to occur when SST anomalies in the Niño1+2 (N1+2) region are becoming neutral/positive at the end of January/mid February while at the same time, cold LN conditions intensify in the central Pacific (Fig. 3). While SST is below average until the end of January in both regions (N1+2 and N3.4), N1+2 starts to warm up at the beginning of February, with

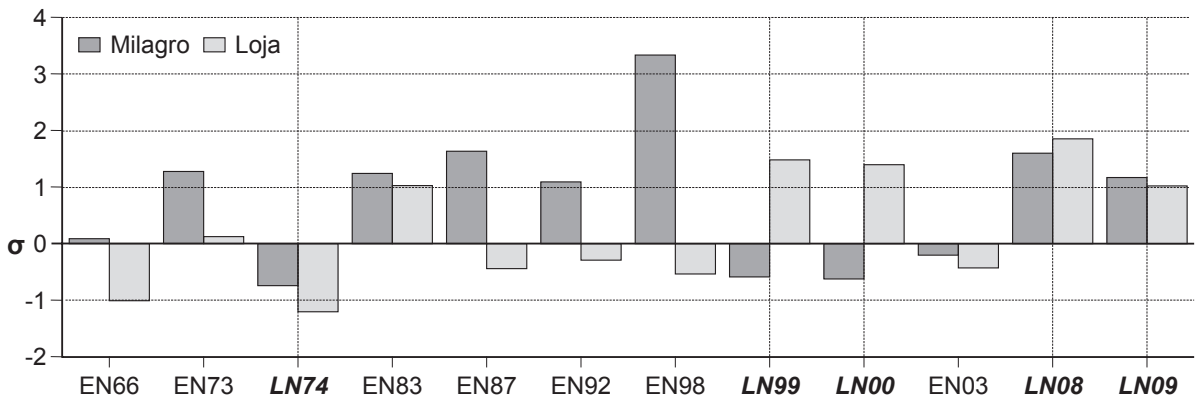

Fig. 2: Rainfall anomalies (in terms of standard deviation σ) for El Niño (EN) and La Niña (LN) events in the coastal plain (meteorological station Milagro) and the Andean highland region (meteorological Station Loja) of southern Ecuador. The anomalies are calculated for the main EN/LN seasons (January to April), with exception of 2009 (January only)

Tab. 1: Rainfall anomalies (in terms of standard deviation σ) for El Niño (EN) and La Niña (LN) events in the coastal plains and the Andean highland region of southern Ecuador (nd: no data available)

	Coast			Highland	
	Guayaquil 4 m a.s.l.	Machala 4 m a.s.l.	Cariamanga 1,960 m a.s.l.	Catamayo 1,230 m a.s.l.	Saraguro 2,525 m a.s.l.
EN66	0.003	-0.347	-0.522	-1.622	-1.35
EN73	1.274	-0.102	0.019	1.116	-0.93
LN74	-0.955	-0.657	-0.343	0.919	0.43
EN83	3.179	3.556	1.507	nd	0.112
EN87	2.036	0.453	-0.489	-1.105	-0.751
LN88	-0.961	-0.626	-0.267	0.196	0.22
EN92	0.74	1.494	-0.718	-0.782	-0.929
EN98	4.25	3.27	2.196	-0.845	-0.246
LN99	-1.096	-0.05	1.295	0.785	1.551
LN00	-1.08	-0.074	1.052	1.458	0.265
EN03	-1.447	-0.801	-0.613	0.874	-0.842
LN08	1.184	0.915	1.85	2.059	0.569

two peaks, at the end of February and the end of March with average positive anomalies of >1 °C. It is striking that the first stronger rain events at the coast (Milagro, 69.2 mm on 28 Jan = +8.1 *σ*) coincide with SSTs converging to 26 °C. While SSTs in the N1+2 region further increase in February by developing coastal EN-like conditions, N3.4-SSTs cool down, generating a central Pacific LN with lowest temperatures in the middle of February. The SST difference between the eastern and central Pacific peaks at the transition from February to March. The first devasting rain event hit the coastal area mid February when average SSTs in the N1+2 region reach 26–27 °C (rainfall Milagro 104 mm on 15 Feb = +12.9 *σ*), followed by the first strong rainfall events in the highlands (Loja 37.8 mm on 17 Feb = +17.0 *σ*, 41.8 mm on 26 Feb=+19.0 *σ*), which coincide with increasing SST differences between the cold Niño3.4 (N3.4) and warm N1+2 region. At the beginning of March, highest positive SST anomalies in the eastern tropical Pacific (N1+2) eventually lead to a second period of severe precipitation and flooding in the coastal parts of southern Ecuador (116 mm at Milagro on 2 Mar = +14.6 *σ*), continuing until mid of March (106 mm at Milagro on 18 Mar = +13.3 *σ*). The whole period from mid February to mid March is also characterized by recurring strong rain events in the highlands at Loja, partly in phase (e.g., 2 March) but mostly out of phase (e.g., 26 Feb, 9 and 13 Mar) with a rainfall peak in the coastal plains.

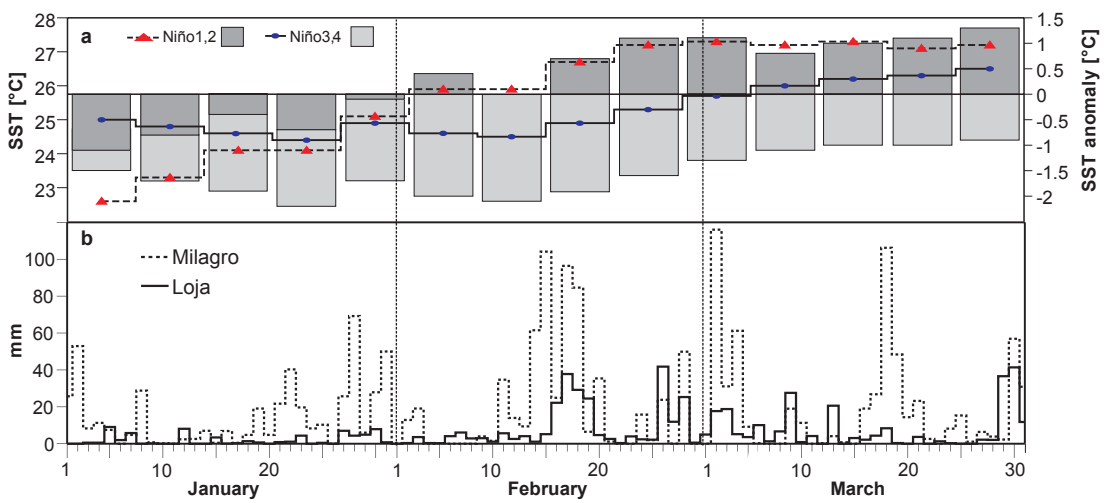

Fig. 3: (a) Weekly averages of sea surface temperature SST (lines) and SST anomalies (bars) in the eastern (Niño1+2 region) and central (Niño3.4 region) tropical Pacific and (b) daily rainfall amounts for the coast (Milagro) and the highlands (Loja) of southern Ecuador J-M 2008. Note that average daily rainfall in the period J-M is 10.6 mm (σ = 7.2 mm) at Milagro (1964-2006) and 3.9 mm (σ = 2.0 mm) at Loja

A final extraordinary rainfall event in the highlands of South Ecuador occurred at the end of March and destroyed the main connection road between Loja and the Catamayo airport (36.6/41.4 mm at Loja on 30/31 Mar = +16.4/18.8 σ).

3.3 SST pattern during periods of exceptional positive rainfall anomalies

To understand the atmospheric processes for the major days of heavy rainfall, spatial SST fields are analysed in more detail. The weekly SST maps for the periods of heavy rainfall are displayed in figure 4. The SST maps show temperature values between 18 and 30 °C as well as a signature for permanent cloudy areas in which SSTs could not be determined because of a permanent cloud cover during the week. With regard to deep convective rainfall, the SST directly off the coast in the N1+2 region coincides best with precipitation in the coastal plains (e.g., Bendix et al. 2000). Several studies emphasized that the SST-threshold for the formation of deep convection is 26 °C, due to the exponential relationship between temperature and evaporation (Graham and Barnett 1987; Waliser and Graham 1993; Zhang 1993). A SST of around 28 °C was proven to trigger exceptional deep convection (Gadgil et al. 1984; Waliser 1996a; Bendix and Bendix 2006) while at SSTs >29.5 °C, a rapid decrease of convective activity is observed. SSTs of 30 °C are found to generate only the same convection rate as at SSTs of 22 °C (Waliser and Graham 1993; Waliser 1996a, b). Moreover, model studies have proven that, in comparison to the absolute SST-value, horizontal SST-gradients are of focal importance as a trigger of deep convection (Lau et al. 1997; Bony et al. 1997; Tompkins and Craig 1999; Tompkins 2001). This is of special interest for the northern boundary of the Peru Current's upwelling area close to southern Ecuador where it is most likely that warm water of the N2 regions encounters cold water of the N1 region under EN conditions. For the first exceptional rain period at the coast (SST map 10–17 Feb), figure 4a reveals that both criteria for deep convection, SSTs > 26 °C at the coastline close to Milagro and horizontal SST gradients particularly in the Gulf of Guayaquil (GoG, 22–26 °C), are met. The highest SST is observed in the GoG, partly reaching values of 28°C. In the N3 area, cold water with SST <20 °C is located in the western part while the eastern region has higher temperatures.

The severe rainfall in the highlands at the end of February and the second phase of heavy precipitation in the coastal area (SST composite 26 Feb to 4 Mar, Fig. 4b) are concomitant with the most pronounced increase of SSTs in the N3 region in the second half of February. This confirms the finding of Vuille et al. (2000) that highland precipitation is particularly sensitive to SSTs in the N3 region where the eastern part in this transition from February to March is warmer than the N1+2 region. As during the first phase of heavy rainfall at the coast, the GoG reveals high SST values with marked SST gradients to the water off the shoreline on a smaller scale. In comparison to the first phase, SSTs in the north-eastern equatorial Pacific are generally enhanced and the cold upwelling directly at the coastline of northern Peru has retreated southwards to ~12°S.

By mid March (SST composite 13-20 Mar, Fig. 4c) heavy rainfall predominantly occurs in the coastal plains, while at the same time declines in the highlands. This situation coincides with a clear cooling in the western and central part of the N3 region. While in the GoG and the adjacent coastline high SSTs >26, but <28°C prevail, the cold upwelling has moved back north to the coast of northern Peru (~6°S).

At the end of March (SST map 23 Mar – 5 Apr, Fig. 4d), SSTs rise in the entire N3 area while at the same time, the highest SSTs are reached off the coast of Costa Rica. The cold upwelling at the north Peruvian coast produces an area of colder offshore water running parallel to the Ecuadorian and Columbian coast. This line generates local SST gradients, particularly to the warm GoG water close to the most affected region around Milagro and Guayaquil. The clearly enhanced N3 SST, which is particularly warmer in the eastern part compared to the N1+2 region, might be responsible for the devasting rainfall event in the highlands. At the same time, the SST gradients close to the coast of southern Ecuador and the GoG are suspected to generate stronger rainfall events at the coast with precipitation amounts of >150 mm for the period between 23 March and 5 April.

3.4 Atmospheric circulation during periods of exceptional positive rainfall anomalies

With regard to the overturning zonal Walker circulation in the tropical Pacific, EN events have been proven to reveal clear westerly wind anomalies in the N3.4 region, while LN is generally associated with easterly wind anomalies in the lower troposphere and the reverse flow in the higher troposphere (Clarke and van Gorder 2003). The wind situation in the

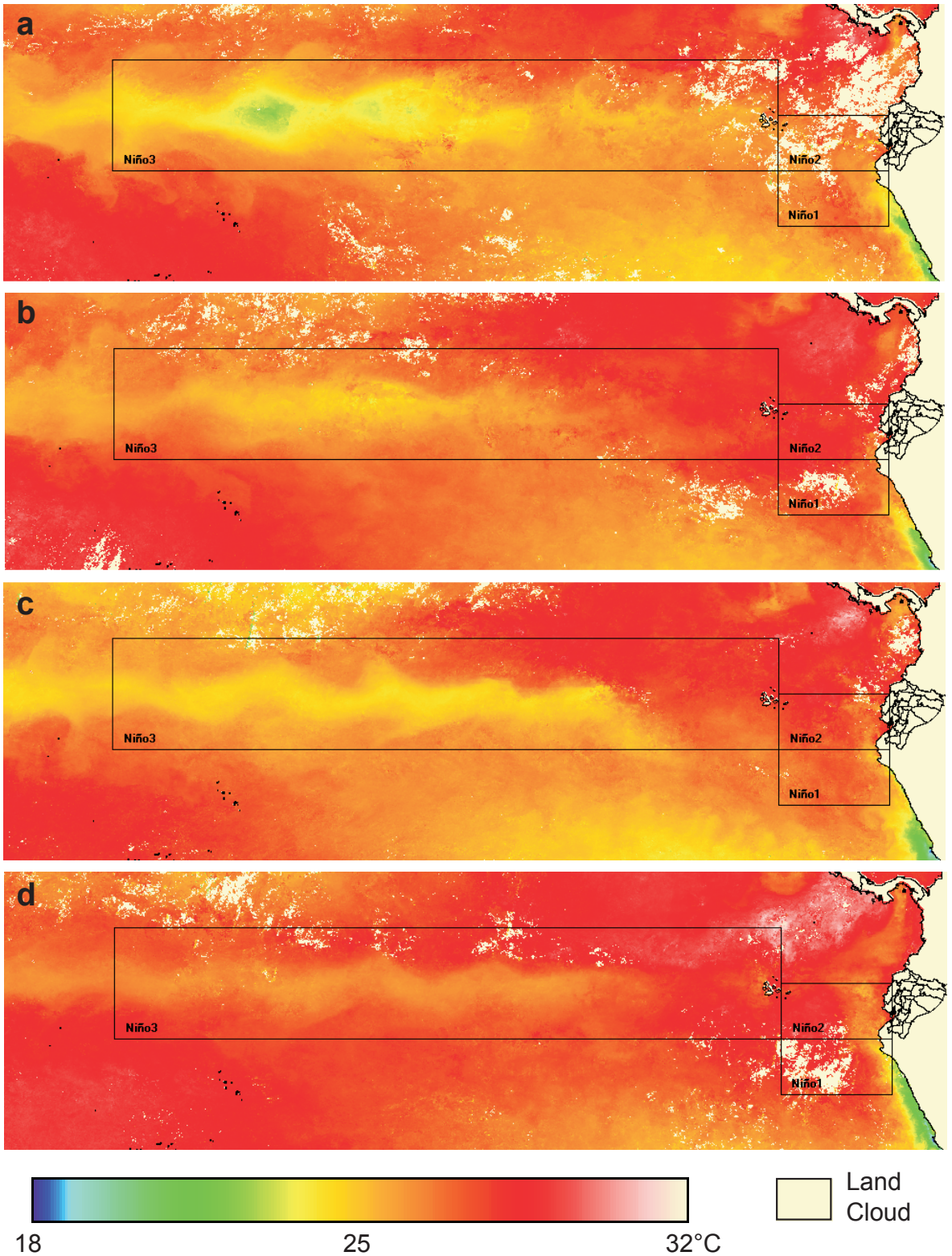

Fig. 4: MODIS weekly SST maps of the N1+2 and N3 region for the weeks of heavy rainfall (a) 10–17 Feb 2008, (b) 26 Feb –4 Mar 2008, (c) 13–20 Mar 2008 and (d) 29 Mar–4 Apr 2008

eastern tropical Pacific is more complex. Murphree and Reynolds (1995) show for the 1989 LN and 1992 EN events that the meridional wind component in the lower troposphere dominates with S (NW) elements during EN (LN). For the 2008 LN event, simulated wind field patterns show distinct regional circulation patterns for all periods of heavy rainfall, which clearly modulate the spatial occurrence and extent of the precipitation fields.

Figure 5 shows the relative frequency of (i) cold, potentially rain bearing clouds, (ii) simulated cumulative precipitation and (iii) measured rainfall at the study area in the Andes of southeastern Ecuador for the three main devastating precipitation events in 2008. The first event of heavy rainfall on 15 February 2008 reveals a typical rainfall distribution for the onset of the significantly enhanced rainy season during El Niño situations (Bendix 2000b). The main simulated rainfall is located over the GoG, affecting the adjacent coastal plains (and thus, the station Milagro) (Fig. 5, left). Heavy rainfall generally extends to the lower parts of the western Andean slopes but does not reach the highlands and the eastern Andean slopes. The cloud frequency map generally confirms the main simulated rainfall area in the coastal plains. However, the small simulated rain area close to the south-eastern Ecuadorian border is not marked by high cloud frequencies. The inspection of single GOES images (not shown here) reveals that a convective cloud cluster forms at 00:00 LST close to Guayaquil remaining stationary with a cold core (231 K) over the GoG up to 17:00 LST. This typical feature can be explained by the high SSTs in the GoG and the concave shape of the coastline, which fosters confluence of nocturnal land breeze, initiating deep convection over the exceptional warm water in the gulf (Bendix 2000b). The event

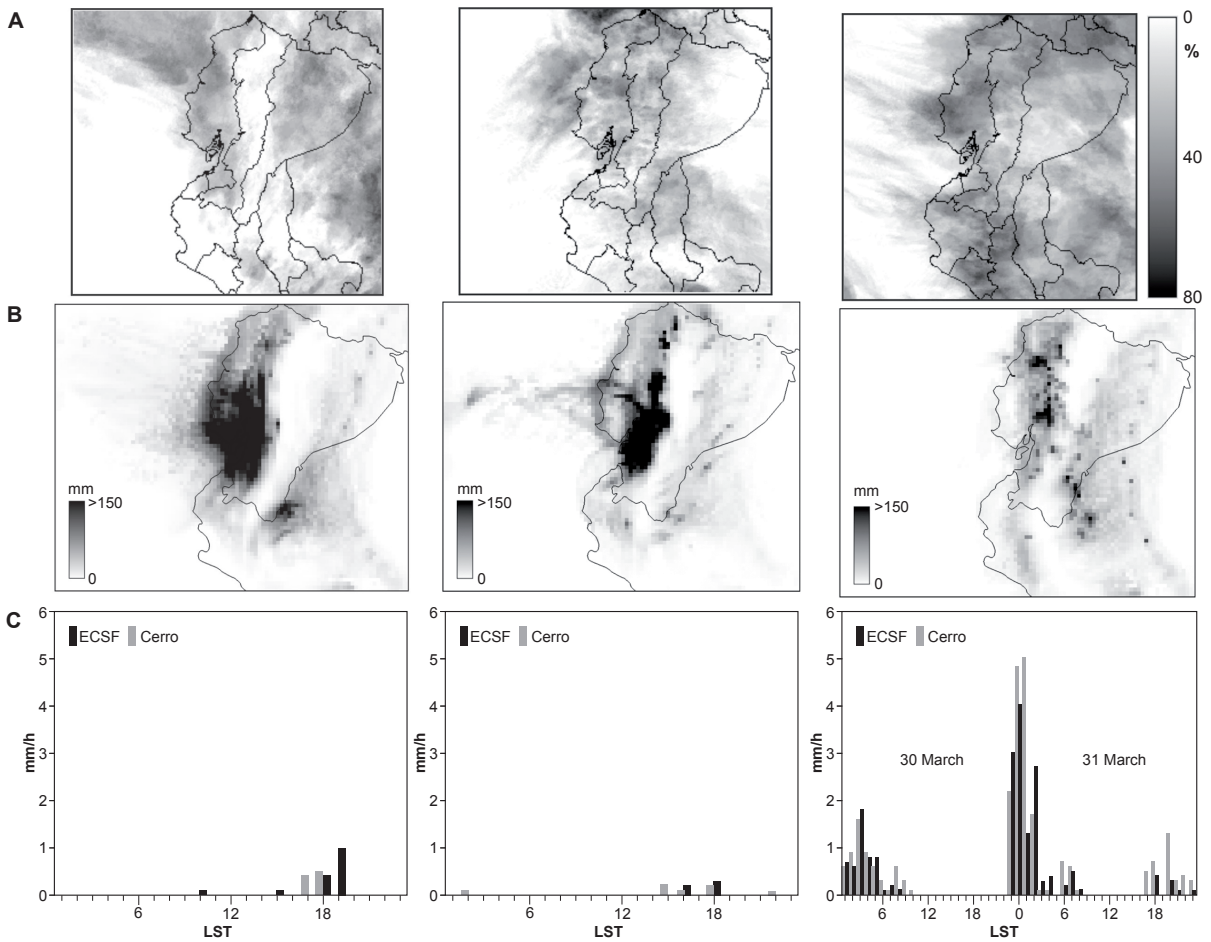

Fig. 5: (a) Frequency of GOES brightness temperatures <255 K for (left) 15 February 2008, (centre) 2 March 2008 and (right) 30 March 2008, (b) Simulated accumulated rainfall of domain 2 for (left) 15 February 2008, (centre) 2 March 2008 and (right) 30 March 2008, and (c) diurnal course of precipitation at the eastern Andean slopes (ECSF and ECSF-Cerro present weather sensors) for the same periods

on 2 March slightly differs from the situation in mid February. Heavy rainfall mainly occurs along the western foothills of the Andean cordillera, particularly in central and southern Ecuador. While the station Milagro close to the GoG experiences the strongest rainfall of the whole event, the eastern Andean escarpment is not affected by heavy precipitation (Fig. 5, centre). The spatial structure of the simulated rain area is confirmed by the cold cloud frequency map. Single GOES IR slots (not shown) point to clear convective activity over the GoG and the western Andean slopes between 22:00 LST (1 Mar) and 03:00 LST (2 Mar). The third situation leading to severe flooding and landslides in the highland of southern Ecuador by the end of March 2008 is completely different compared to the other two events. It is mainly characterized by more isolated but intensive cellular convection. The simulated rainfall map for 30 March reveals moderate to strong precipitation along the western and the eastern escarpment of the Andes and scattered isolated centres of heavy rainfall including the highland area of southern Ecuador around Loja (Fig. 5, right). Even the eastern escarpment receives strong rainfall during 30–31 March, particularly in the early morning hours. Also the cloud frequency map reveals high cloudiness with partly cellular extension in the area of the eastern slopes of the south Ecuadorian Andes.

Figure 6 illustrates the circulation patterns related to the three heavy rainfall events. On 15 February 2008, the simulated 925 hPa wind field shows the typical characteristics of EN events with southerly winds crossing the equator in the eastern Pacific. The coastal waters off the coast of Ecuador and the GoG are in the centre of a low level clockwise vortex, which is situated more west in the upper troposphere (300 hPa) (Fig. 6, upper left). At the eastern boundary of the N3 region, the wind field is characterized by anti-clockwise vortex flow in both atmospheric levels, which is related to the LN-cold pool that reaches the eastern edge of the N3 region (Fig. 4a). The atmospheric instability in the transition zone of the N3 and N2 regions due to the distinct SST gradients leads to deep convection, which endures for several days in the area, indicated in the SST maps of figure 4 by the white cloud signature. In the GoG, the high SSTs at the direct coastline (maximum is 28°C in front of Guayaquil and Milagro, see fig. 4a), as well as extremely strong SST gradients (some neighbouring pixels record values between 21 and 26°C), contribute to the strong

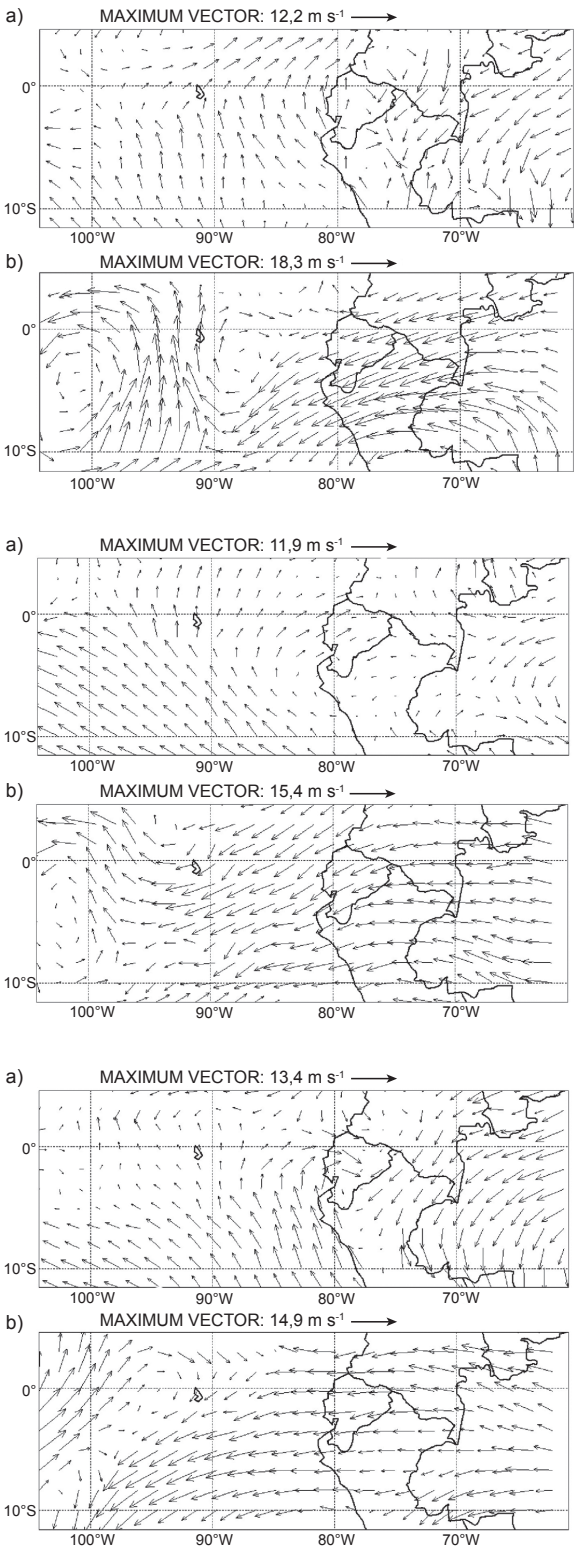

Fig. 6: (a) Simulated wind field of domain 1 at 925 hPa and (b) 300 hPa for 09.00 LST on (upper left) 15 Feb 2008, (upper right) 02.00 LST on 2 Mar 2008 and (lower left) 05.00 LST on 30 Mar 2008

rainfall event that covers the whole coastal area of southern Ecuador up to the Peruvian border. Like the rainfall patterns, the atmospheric circulation of the second event (2 March) reveals only slight differences, particularly in the lower troposphere (925 hPa). The winds at the 925 hPa level generally depict the same southerly direction typical for EN conditions, but with a more intense clockwise vortex circulation over Ecuador, which might be triggered by the clearly enhanced SSTs off the coast of northern Peru (Fig. 4b). This intensification provides continuous moisture flow to the western slopes of the Andes, where forced convection eventually leads to the formation of heavy rainfall. In the upper troposphere, easterlies are well-established until long. ~95°W. The third period with differing rainfall patterns is characterised by deviating circulation patterns. The low level wind field (925 hPa) depicts that the clockwise vortex is shifted to north Peru with a greater extensions of the area of minimum wind velocity ranging from the coastal waters towards the Andes and the adjacent eastern Amazon. Even if the wind field over the coastal waters off the coast of Ecuador is dominated by weak south-westerly winds, the south-eastern Ecuadorian Andes are already characterised by LN-like north-easterly to north-westerly winds (also confirmed by wind observations). Upper air circulation reveals well-developed easterlies until long. ~100°W, where an anti-clockwise vortex circulation is displayed over the eastern edge of the N3 region. Especially the western N1 region shows strong convection during the whole week (white cloud area in SST map Fig. 4d).

The vertical circulation and the atmospheric humidity fields during the three events are displayed in figure 7 along a cross-section through southern Ecuador (lat. 3°S). For the event on 15 Feb (Fig. 7, top), a well-established updraft area is found over the whole Andes. However major updraft and moist convection with saturation conditions up to the 400 hPa level are simulated, starting at the western Andean slopes, extending to the coastal plains of southern Ecuador. Similar circulation patterns can be observed for 2 March with the major updraft area over the western escarpment of the Andes. However, deep saturation is not as horizontally and vertically extended as in the first period (Fig. 7, centre). Figure 7 (bottom) points out that the third period on 30 March is characterized by a completely different situation. The main updraft area is located at the eastern escarpment of the Andes reaching up to the 200 hPa level. The upward motion is accompanied by deep moisture saturation conditions up to the 400 hPa level, responsible for the heavy rainfall events in the Andes.

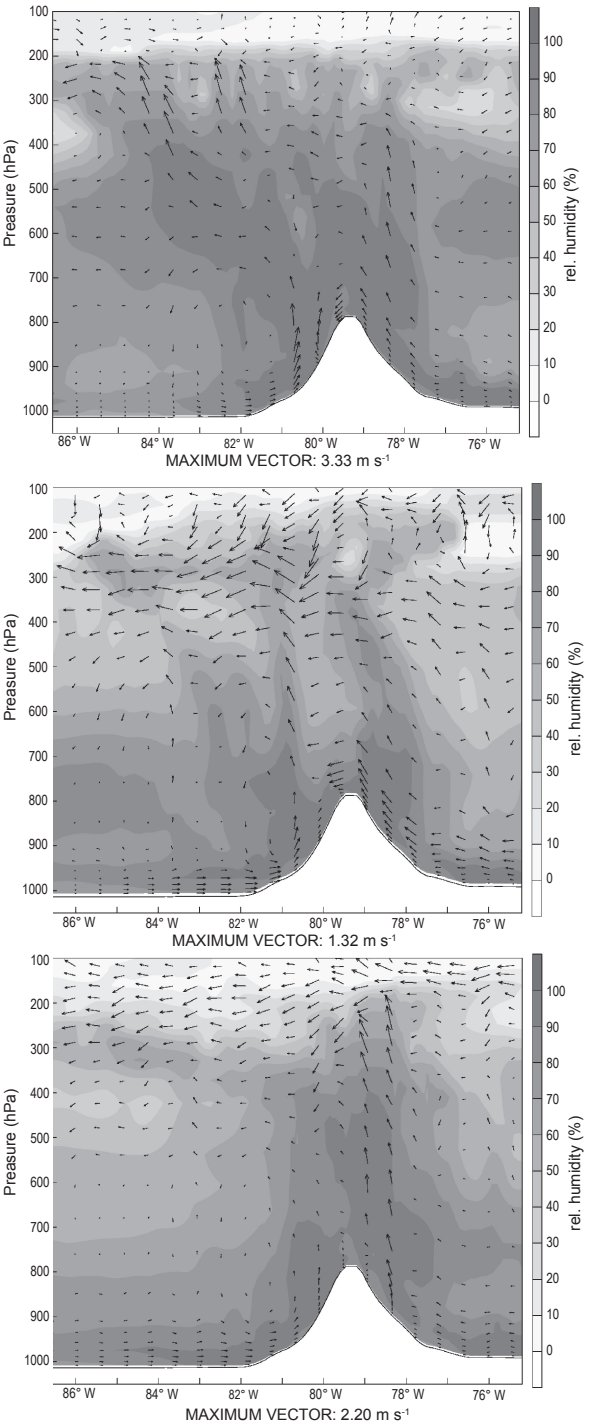

Fig. 7: Simulated vertical flow and relative humidity for (top) 09.00 LST on 15 Feb 2008, (centre) 02.00 LST on 2 Mar 2008 and (bottom) for 05.00 LST on 30 Mar 2008. The profiles are taken from domain 2 at Lat. 3°S (southern Ecuador)

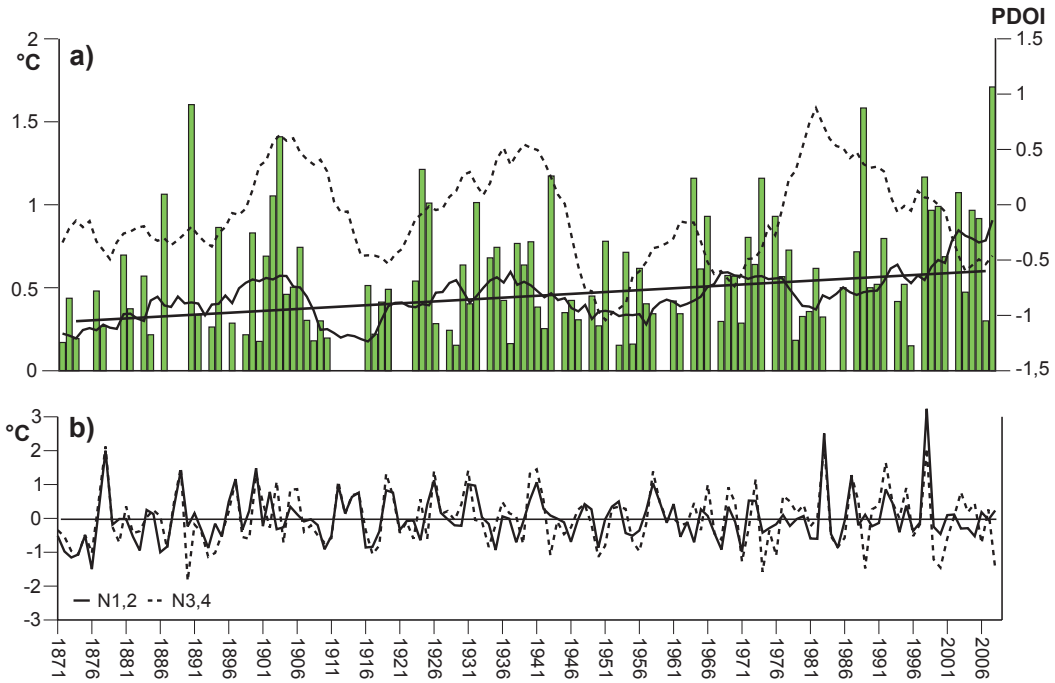

Fig. 8: (a) Absolute SST anomaly difference between the eastern and central tropical Pacific (|Niño1+2 – Niño3.4|) (bars), 11-year moving average (black curve) and trend (black line) (average January–April). 11-year moving average of the PDO index (dotted line) (average January–April) where positive (negative) numbers represent a PDO warm (cold) phase (b) SST-anomalies for the Niño1+2 and 3.4 regions (average January–April)

4 Discussion and conclusions

The analysis of the course of the 2008 LN event in the N3 and N1+2 region, and the traditional EN area of southern Ecuador, confirms that EN conditions in the eastern tropical Pacific can prevail even if the central Pacific exhibits LN cold pool conditions. With regard to the generation of heavy rainfall in the central El Niño area of southern Ecuador, it has turned out that EN and LN-like rainfall events can occur under these specific conditions concurrently in one rainy season where the first situations mostly affect the western Andean slopes and the coastal plains, while the latter shows main impacts in the highlands and the eastern escarpment of the Andes.

It should be stressed that the 2008 situation is not the first time that rainfall anomalies in South Ecuador do not render the traditional central Pacific ENSO (and thus SOI) behaviour, which means that cold (warm) events bring higher (lower) precipitation to the coastal part of Ecuador and vice versa for the Andean highlands. Since the beginning of the 21st century, central Pacific warm events (e.g., 2002-2005) have been partly characterized by below-average rainfall in the traditional EN area of southern Ecuador (Bendix and Bendix 2006). Thus, the 2008 central Pacific LN event is only the latest example of anomalous teleconnections in the tropical Pacific. However, the question arises as to the mechanism that induces this rapid change in the current century and if it is due to natural variability or a signal of global climate change.

By inspecting time series of tropical Pacific SST anomalies (Fig. 8) as one major trigger of the zonal overturning circulation in the tropical Pacific, it is evident that 2008 is the year with the highest SST anomaly difference between the eastern (N1+2 region) and the central tropical (N3.4 region) Pacific since 1871 (Fig. 8a). Additionally, the 11-year moving average points to a general increase of this difference, which is particularly intensified at the beginning of the current century. For almost all of the past centuries, the direction of the temperature anomaly in the central and eastern tropical Pacific has been consistent. Since 2000, the SST anomalies of both regions have been predominantly out of phase (Fig. 8b), the main reason for the greater differences between the central and eastern tropical Pacific, and the impact mode change in the traditional El Niño region of southern Ecuador.

The observed change could be a signal of global warming, which is already evident in the tropical Pacific-South American region (Vuille et al.

2003). Model studies reveal that global warming would affect the tropical eastern Pacific more than the central-western part (Vecchi and Soden 2007; Latif and Keenlyside 2008). One major expected effect is the weakening of the trades and the south Pacific anticyclone that is moving southwards (Vecchi et al. 2006). This might lead to lower intensities of the cold upwelling off the South American tropical west coast, associated with an increase of SSTs and atmospheric updraft conditions in the N1+2 region (Vecchi and Soden 2007). Furthermore, palaeodata suggest that the Innertropical Convergence Zone (ITCZ) is shifted southward during periods of CO_2-driven warming (Toggweiler 2009). All these effects could intensify the circulation patterns of the normal rainy season in southern Ecuador, where the southward shift of the ITCZ brings warm equatorial surface water with north-westerly low level wind stress to the coast of southern Ecuador and northern Peru during January to April, which leads to atmospheric instability and rainfall. Convective rainfall and thunderstorms in the highlands at Loja are known to be related to westerly wind anomalies in this season (Bendix and Lauer 1992). Consequently, above normal SSTs in the N1+2 region that are associated with westerly wind anomalies could generally mean El Niño-like rainfall conditions in both areas of the traditional El Niño region (as 2008) while a central Pacific LN prevails. Additionally, the observed novel SST-anomaly dipole pattern should intensify the zonal Walker circulation and its updraft branch over southern Ecuador due to an increase of the thermal asymmetry between the N1+2 and particularly the N3 region as seen in the current study. On the other hand, the weakening of an ENSO-driven EN situation (as 2002 and 2005; for 2002 see also McPhaden 2004) could be a result of a reduced thermal asymmetry between eastern and western Pacific. Thus, a weakening of the Walker circulation and its updraft branch in the N1+2 region might occur. This could lead to below normal precipitation as observed for the weak EN situations in the current century, but also an eastward shift of convection (Vecchi and Soden 2007), which could lead to a propagation of Pacific instability across the Andes (as end of March 2008).

However, EN/LN circulation patterns in the tropical Pacific also interact with the background signal of the Pacific Decadal Oscillation (PDO). In a PDO warm phase, the north Pacific anticyclone is shifted towards the western north Pacific, which facilities the wind-driven transport of warm equatorial water to the N3.4 region. This would favour the development of ENSO-driven EN conditions. In a PDO cold phase, the N-Pacific anticyclone is shifted eastwards, thus boosting the impact of occurring LN conditions in the N3.4 region while at the same time moderating the effect of emerging central Pacific EN events. Additionally, the eastern position of the anticyclone during a PDO cold phase fosters the shallow meridional overturning circulation in the eastern Pacific, particularly dominant during the rainy season in southern Ecuador (J-A). The well-developed EN events in the 80s and 90s of the last century, encompassing both strong events in 1983 and 1998, were accompanied by a PDO warm phase, which supports the interrelation between ENSO and PDO. The strong LN 1999 marked the onset of a PDO cold phase that could generally explain the weak EN and strong LN intensities at the beginning of the century. To summarize, the observed novel constellation of EN in the N1+2 region accompanied by strong LN conditions in the N3.4 region could be also the result of a PDO cold phase that induces similar atmosphere-ocean circulation patterns in the tropical Pacific as expected from global warming. However, SST data show that the decoupled N1+2 and N3.4 anomalies of the 2008 event have not occurred during previous PDO cold phases and it is striking that PDO and SST anomaly difference oscillations are out of phase at the end of the 60s of the last century (Fig. 8a). Even if no sound estimate of climate change effects on PDO is hitherto available, it can be concluded that the novel situation with the dipole structure of SST anomalies in the central and eastern tropical Pacific in connection with exceptional EN-like rainfall anomalies in the traditional El Niño region of southern Ecuador must be due to a combination of long-term natural variability (PDO) and a climate change signal. At this time, it is not possible to decide which signal has the major impact. Future studies are needed to disentangle the effect of climate change on PDO and its relation to ENSO regimes and severe flood/drought events in the tropical Pacific land areas. The general lesson learnt is that central Pacific SST and the SOI are becoming more unreliable indicators for the SST and rainfall situation in the N1+2 region, and the traditional EN area of southern Ecuador and northern Peru, particularly in PDO cold phases under climate change.

Acknowledgements

The authors are indebted to the German Research Foundation (DFG) for the funding of the work in the scope of the Research Unit RU816 '*Biodiversity and Sustainable Management of a Megadiverse Mountain Ecosystem in South Ecuador*' (BE 1780/15-1 and 15-2). We also would like to thank the foundation Nature & Culture International (NCI) Loja and San Diego as well as the Ecuadorian Ministry of Environment (MAE) for logistic support.

References

An, S.-I.; Ham Y.-G.; Kug J.-S.; Jin F.-F. and Kang, I.-S. (2005): El Niño–La Niña asymmetry in the Coupled Model Intercomparison Project simulations. In: J. Climate 18 (14), 2617–2627. DOI: 10.1175/JCLI3433.1

Barnett T.; Graham, N.; Cane, M.; Zebiak, S.; Dolan, S.; O'Brien, J. J. and Legeler, D. (1988): On the prediction of the El Niño of 1986–1987. In: Science 241, 192–196. DOI: 10.1126/science.241.4862.192

Beck, E.; Makeschin, F.; Haubrich, F.; Richter, M.; Bendix, J. and Valerezo, C. (2008): The ecosystem (Reserva Biologica San Francisco). Ecological Studies 198. Berlin, 1–13.

Bendix, A. and Bendix, J. (2006): Heavy rainfall episodes in Ecuador during El Niño events and associated regional atmospheric circulation and SST patterns. In: Adv. Geosci. 6, 43–49. DOI: 10.5194/adgeo-6-43-2006

Bendix, J. (2000a): A comparative analysis of the major El Niño events in Ecuador and Peru over the last two decades. In: Zbl. Geol. Paläontol. Teil I 1999-7/8, 1119–1131.

– (2000b): Precipitation dynamics in Ecuador and Northern Peru during the 1991/92 El Niño – A remote sensing perspective. In: Int. J. Remote Sens. 21, 533–548. DOI: 10.1080/014311600210731

Bendix, J. and Beck, E. (2009): Spatial aspects of ecosystem research in a biodiversity hot spot of southern Ecuador – an introduction. In: Erdkunde 63, 305–308. DOI: 10.3112/erdkunde.2009.04.01

Bendix, J. and Bendix, A. (1998): Climatological aspects of the 1991/92 El Niño in Ecuador. In: Bull. de L'Institut Francais d'Études Andines 27, 655–666.

Bendix, J. and Lauer, W. (1992): Rainy seasons of Ecuador and their climate-dynamic interpretation. In: Erdkunde 46, 118–134. DOI: 10.3112/erdkunde.1992.02.04

Bendix, J.; Bendix, A., and Richter, M. (2000): El Niño 1997/1998 in northern Peru: an indication for a change of the ecosystem? In: Peterm. Geogr. Mitt. 144 (4), 20–31.

Bendix, J.; Gämmerler, S.; Reudenbach, C. and Bendix, A. (2003): A case study on rainfall dynamics during El Niño/La Niña 1997/99 in Ecuador and surrounding areas as inferred from GOES-8 and TRMM-PR observations. In: Erdkunde 57, 81–93. DOI: 10.3112/erdkunde.2003.02.01

Bendix, J.; Rollenbeck, R. and Palacios, E. (2004): Cloud classification in the tropics – a suitable tool for climate-ecological studies in the high mountains of Ecuador. In: Int. J. Remote Sens. 25, 4521–4540. DOI: 10.1080/01431160410001709967

Bendix, J.; Rollenbeck, R. and Reudenbach, C. (2006a): Diurnal patterns of rainfall in a tropical Andean valley of southern Ecuador as seen by a vertically pointing K-band Doppler radar. In: Int. J. Climatol. 26, 829–846. DOI: 10.1002/joc.1267

Bendix, J.; Rollenbeck, R.; Göttlicher, D. and Cermak, J. (2006b): Cloud occurrence and cloud properties in Ecuador. In: Clim. Res. 30, 133–147. DOI: 10.3354/cr030133

Bendix, J.; Rollenbeck, R.; Fabian, P.; Emck, P.; Richter, M. and Beck, E. (2008): Climate variability. Ecological Studies 198. Berlin, 280–291.

Bendix, J.; Behling, H.; Peters, T.; Richter, M. A. and Beck, E. (2010): Functional biodiversity and climate change along an altitudinal gradient in a tropical mountain rainforest. In: Tscharntke, T.; Leuschner, C.; Veldkamp, E.; Faust, H.; Guhardja, E. and Bidin, A. (eds.): Tropical rainforests and agroforests under global change. Berlin, 239–268.

Bony, S.; Lau, K.-M. and Sud, Y. C. (1997): Sea surface temperature and large-scale circulation influences on tropical greenhouse effect and cloud radiative forcing. In: J. Climate 10, 2055–2076. DOI: 10.1175/1520-0442(1997)010<2055:SSTALS>2.0.CO;2

Cane, M. A. (1991): Forecasting El Niño with a geophysical model. In: Glantz, M. H.; Katz, R. W. and Nicholls, N. (eds.): Teleconnections linking worldwide climate anomalies. Cambridge, 345–370.

Cermak J.; Bendix, J. and Dobbermann, M. (2008): FMet – an integrated framework for Meteosat data processing for operational scientific applications. In: Comp. Geosci. 34, 1638–1644. DOI: 10.1016/j.cageo.2007.12.006

Chen F. and Dudhia, J. (2001): Coupling an advanced land surface-hydrology model with the Penn State-NCAR MM5 modeling system. Part I: Model implementation and sensitivity. In: Mon. Wea. Rev. 129, 569–585. DOI: 10.1175/1520-0493(2001)129<0569:CAALSH>2.0.CO;2

Clarke, A. J. and van Gorder, S. (2003): Improving El Niño predicition using a space-time integration of Ino-Pacific winds and equatorial Pacific upper ocean heat content. In: Geophys. Res. Lett. 30 (7), 1399. DOI: 10.1029/2002GL016673

Dudhia, J. (1989): Numerical study of convection observed during the winter monsoon experiment using a mesoscale two-dimensional model. In: J. Atmos. Sci. 46, 3077–3107. DOI: 10.1175/1520-0469(1989)046<3077:NSOCOD>2.0.CO;2

Douglas, M. W.; Mejia, J.; Ordinola, N. and Boustead, J. (2009): Synoptic variability of rainfall and cloudiness along the coast of northern Peru and Ecuador during the 1997/98 El Niño event. In: Mon. Wea. Rev. 137, 116–136. DOI: 10.1175/2008MWR2191.1

Fedorov, A. V. and Philander, S. G. (2000): Is El Niño changing? In: Science 288, 1997–2002. DOI: 10.1126/science.288.5473.1997

Fries, A.; Rollenbeck, R.; Göttlicher, D.; Nauss, T.; Homeier, J.; Peters, T. and Bendix, J. (2009): Thermal structure of a megadiverse Andean mountain ecosystem in southern Ecuador, and its regionalization. In: Erdkunde 63, 321–335. DOI: 10.3112/erdkunde.2009.04.03

Gadgil, S.; Joseph, P. V. and Joshi, N. V. (1984): Ocean – atmosphere coupling over monsoon regions. In: Nature 312, 141–143. DOI: 10.1038/312141a0

Gemmill, W.; Katz, B. and Li, X. (2007): Daily real-time global sea surface temperature – high resolution analysis at NOAA/NCEP. In: NOAA/NWS/NCEP/MMAB Office Note 260 (available at: http://polar.ncep.noaa.gov/sst/).

Glantz, M. H. (1984): Floods, fires, and famine: is El Niño to blame? In: Oceanus 27, 14–19.

Graham, N. E., and Barnett, T. P. (1987): Sea surface temperature, surface wind divergence, and convection over tropical oceans. In: Science 238, 657–659. DOI: 10.1126/science.238.4827.657

Hong, S.-Y.; Noh, Y. and Dhudia, J. (2006): A new vertical diffusion package with an explicit treatment of entrainment. In: Mon. Wea. Rev. 134, 2318–2341. DOI: 10.1175/MWR3199.1

Kain, J. S., and Fritsch, J. M. (1993): Convective parameterization for mesoscale models: the Kain-Fritsch scheme. Meteorol. Monogr. 24. Boston, 165–170.

Kalnay, E.; Kanamitsu, M.; Kistler, R.; Collins, W.; Deaven, D.; Gandin, L.; Iredell, M.; Saha, S.; White, G.; Woollen, J.; Zhu, Y.; Chelliah, M.; Ebisuzaki, W.; Higgins, W.; Janowiak, J.; Mo, K. C.; Ropelewski, C.; Wang, J.; Leetmaa, A.; Reynolds, R.; Jenne, R. and Joseph, D. (1996): The NCEP/NCAR 40-year reanalysis project. In: Bull. Amer. Meteor. Soc. 77, 437–471. DOI: 10.1175/1520-0477(1996)077<0437:TNYRP>2.0.CO;2

Kerr, R. A. (1999): Does a globe-gridling disturbance jigger El Niño? In: Science 285, 322–323. DOI: 10.1126/science.285.5426.322

Kessler, W. S. (2001): EOF representations of the Madden-Julian Oscillation and its connection with ENSO. In: J. Climate 14, 3055–3061. DOI: 10.1175/1520-0442(2001)014<3055:EROTMJ>2.0.CO;2

Kiladis, G. N. and van Loon, H. (1988): The Southern Oscillation: VII: meteorological anomalies over the Indian and Pacific sectors associated with extremes of the oscillation. In: Mon. Wea. Rev. 116, 120–136. DOI: 10.1175/1520-0493(1988)116<0120:TSOPVM>2.0.CO;2

Latif, M. and Keenlyside, N. S. (2009): El Niño/Southern oscillation response to global warming. In: Proc. Natl. Acad. Sci. 106 (49), 20578–20583. DOI: 10.1073/pnas.0710860105

Lau, K.-M.; Wu, H.-T. and Bony, S. (1997): The role of large-scale atmospheric circulation in the relationship between tropical convection and sea surface temperatures. In: J. Climate 10, 381–392. DOI: 10.1175/1520-0442(1997)010<0381:TROLSA>2.0.CO;2

Lin, Y.-L.; Farley, R. D. and Orville, H. D. (1983): Bulk parameterization of the snow field in a cloud model. In: J. Climate Appl. Meteor. 22, 1065–1092. DOI: 10.1175/1520-0450(1983)022<1065:BPOTSF>2.0.CO;2

McPhaden, M. J. (2004): Evolution of the 2002/03 El Niño. In: Bull. Amer. Meteor. Soc. 85, 677–695. DOI: 10.1175/BAMS-85-5-677

Meehl, G. A.; Teng, H. and Branstator, G. (2006): Future changes of El Niño in two coupled climate models. In: Clim. Dyn. 26, 549–566. DOI: 10.1007/s00382-005-0098-0

Mlawer, E.; Taubmann, S.; Brown, P.; Iacono, M. and Clough, S. (1997): Radiative transfer in inhomogenous atmospheres: RRTM, a valid correlated-k model for the longwave. In: J. Geophys. Res. 102, 16663–16682. DOI: 10.1029/97JD00237

Monin, A. S. and Obukhov, A. M. (1954): Basic laws of turbulent mixing in the ground layer of the atmosphere. In: Akad. Nauk. SSSR, Geofiz. Inst. Trudy 151, 163–187.

Murphree, T., and Reynolds, C. (1995): El Niño and La Niña effects on the northeast Pacific: The 1991–1993 and 1988–1989 events. In: CalCOFI Rep. 36, 45–56.

OCHA (2008a): Situation Report No. 3. Ecuador Floods. United Nations Office for the Coordination of Humaitarian Affairs, Panama.

– (2008b): Situation Report No. 5. Ecuador Floods. United Nations Office for the Coordination of Humaitarian Affairs, Panama

Pavia, E. G.; Graef, F. and Reyes, J. (2006): PDO–ENSO effects in the climate of Mexico. In: J. Climate 16, 6433–6438. DOI: 10.1175/JCLI4045.1

Power, S. B., and Smith, I. N. (2007): Weakening the Walker Circulation and apparent dominance of El

Niño both reach record levels, but has El Niño really changed? In: Geophys. Res. Lett. 34, L18702. DOI: 10.1029/2007GL030854

Rayner, N. A.; Parker, D. E.; Horton, E. B.; Folland, C. K.; Alexander, L. V.; Rowell, D. P.; Kent, E. C. and Kaplan A. (2003): Global analyses of sea surface temperature, sea ice and night marine air temperature since the late nineteenth century. In: J. Geophys. Res. 108 (D14), 4407 DOI: 10.1029/2002JD002670

Reynolds R. W. and Smith, T. M. (1994): Improved global sea surface temperature analyses using optimum interpolation. In: J. Climate 7, 929–948. DOI: 10.1175/1520-0442(1994)007<0929:IGSSTA>2.0.CO;2

– (1995): A high-resolution global sea surface temperature climatology. In: J. Climate 8, 1571–1583. DOI: 10.1175/1520-0442(1995)008<1571:AHRGSS>2.0.CO;2

Richter, M. (2003): Using plant functional types and soil temperatures for eco-climatic interpretation in southern Ecuador. In: Erdkunde 57, 161–181. DOI: 10.3112/erdkunde.2003.03.01

Rollenbeck, R.; Bendix, J.; Fabian, P.; Boy, J.; Dalitz, H.; Emck, P.; Oesker, M. and Wilcke, W. (2007): Comparison of different techniques for the measurement of precipitation in tropical montane rain forest regions. In: J. Atmos. Oceanic Technol. 24, 156–168. DOI: 10.1175/JTECH1970.1

Ropelewski, C. F., and Halpert, M. S. (1987): Global and regional scale precipitation patterns associated with the El Niño/Southern Oscillation. In: Mon. Wea. Rev. 115, 1606–1626. DOI: 10.1175/1520-0493(1987)115<1606:GARSPP>2.0.CO;2

Schoennagel, T.; Veblen, T. T.; Romme, W. H.; Sibold, J. S. and. Cook, E. R (2006): ENSO and PDO variability affect drought-induced fire occurrence in Rocky Mountain subalpine forests. In: Ecol. Appl. 15, 2000–2014.

Smith, T. M. and Reynolds, R. W. (2003): Extended reconstruction of global sea surface temperatures based on COADS data (1854–1997). In: J. Climate 16, 1495–1510. DOI: 10.1175/1520-0442-16.10.1495

– (2004): Improved extended reconstruction of SST (1854–1997). In: J. Clim. 17, 2466–2477. DOI: 10.1175/1520-0442(2004)017<2466:IEROS>2.0.CO;2

Suarez, M. J. and Schopf, P. S. (1988): A delayed action oscillator for ENSO. In: J. Atmosph. Sci. 45, 3283–3287. DOI: 10.1175/1520-0469(1988)045<3283:ADAOFE>2.0.CO;2

Takahashi, K. (2004): The atmospheric circulation associated with extreme rainfall events in Piura, Peru, during the 1997–1998 and 2002 El Niño events. In: Ann. Geophys. 22, 3917–3926. DOI: 10.5194/angeo-22-3917-2004

Takayabu, Y. N.; Iguchi, T.; Kachi, M.; Shibata, A. and Kanzawa, H. (1999): Abrupt termination of the 1997–98 El Niño in response to a Madden-Julian oscillation. In: Nature 402, 279–282. DOI: 10.1038/46254

Toggweiler, J. R. (2009): Shifting westerlies. In: Science 323, 1434–1435. DOI: 10.1126/science.1169823

Tompkins, A. M. (2001): On the relationship between tropical convection and sea surface temperature. In: J. Climate 14, 633–637. DOI: 10.1175/1520-0442(2001)014<0633:OTRBTC>2.0.CO;2

Tompkins, A. M. and Craig, G. C. (1999): Radiative-convective equilibrium in a three-dimensional cloud ensemble model. In: Quart. J. Roy. Met. Soc. 124, 2073–2097.

Trenberth, K. E. and Hoar, T. J. (1996): The 1990–1995 El Niño-Southern Oscillation event: longest on record. In: Geophys. Res. Lett. 23, 57–60. DOI: 10.1029/95GL03602

– (1997): El Niño and climate change. In: Geophys. Res. Lett. 24, 3057–3060. DOI: 10.1029/97GL03092

Trenberth, K. E. and Stepaniak, D. P. (2001): Indices of El Niño evolution. In: J. Climate 14**,** 1697–1701. DOI: 10.1175/1520-0442(2001)014<1697:LIOENO>2.0.CO;2

Vecchi, G. A. (2008): Examining the tropical Pacific's response to global warming. In: EOS 89, 81–83.

Vecchi, G. A. and Soden, B. J. (2007): Global warming and the weakening of the tropical circulation. In: J. Climate 20, 4316–4340. DOI: 10.1175/JCLI4258.1

Vecchi, G. A.; Soden, B. J.; Wittenberg, A. T.; Held, I. M.; Leetmaa, A. and Harrison, M. J. (2006): Weakening of the tropical Pacific atmospheric circulation due to anthropogenic forcing. In: Nature 441, 73–76. DOI: 10.1038/nature04744

Vuille, M.; Bradley, R. S. and Keimig, F. (2000): Climate variability in the Andes of Ecuador and its relation to tropical Pacific and Atlantic sea surface temperature anomlies. In: J. Climate 13, 2520–2535. DOI: 10.1175/1520-0442(2000)013<2520:CVITAO>2.0.CO;2

Vuille, M.; Bradley, R. S.; Werner, M. and Keimig, F. (2003): 20th century climate change in the tropical Andes: observations and model results. In: Climatic Change 59, 75–99. DOI: 10.1023/A:1024406427519

Waliser, D. (1996a): Climate controls on high sea surface temperatures. In: World Res. Rev. 8, 289-310.

– (1996b): Formation and limiting mechanisms for very high sea surface temperature: linking dynamics and the thermodynamics. In: J. Climate 9, 161–188. DOI: 10.1175/1520-0442(1996)009<0161:FALMFV>2.0.CO;2

Waliser, D. E. and Graham, N. E. (1993): Convective cloud systems and warm-pool SSTs: coupled interactions and self-regulation. In: J. Geophys. Res. 98, 12881–12893. DOI: 10.1029/93JD00872

Waliser, D.; Lau, K. M.; Stern, W. and Jones, C. (2003): Potential predictability of the Madden-Julian Oscillation. In: Bull. Amer. Meteor. Soc. 84, 33–50. DOI: 10.1175/BAMS-84-1-33

Walton, C. C.; Pichel, W. G. and Sapper, J. F. (1998): The development and operational application of nonlinear algorithms for the measurement of sea surface temperatures with the NOAA polar-orbiting environmental satellites. In: J. Geophys. Res. 103 (C12), 27,999–28,012. DOI: 10.1029/98JC02370

Wicker, L. J. and Skamarock, W. C. (2002): Time splitting methods for elastic models using forward time schemes. In: Mon. Wea. Rev. 130, 2088–2097. DOI: 10.1175/1520-0493(2002)130<2088:TSMFEM>2.0.CO;2

Wolter, K. and Timlin, M. S. (1998): Measuring the strength of ENSO events – how does 1997/98 rank? In: Weather 53, 315–324.

Wyrtki, K. (1975): El Niño – the dynamic response of the equatorial Pacific ocean to atmospheric forcing. In: J. Phys. Oceanogr. 5, 572–584. DOI: 10.1175/1520-0485(1975)005<0572:ENTDRO>2.0.CO;2

Zhang, C. (1993): Large-scale variability of atmospheric deep convection in relation to sea surface temperature in the tropics. In: J. Climate 6, 1898–1913. DOI: 10.1175/1520-0442(1993)006<1898:LSVOAD>2.0.CO;2

Zebiak, S. E. and Cane, M. A. (1987): A model of El Niño-Southern Oscillation. In: Mon. Wea. Rev. 115, 2262–2278. DOI: 10.1175/1520-0493(1987)115<2262:AMENO>2.0.CO;2

Authors

Prof. Dr. Jörg Bendix
Astrid Bendix
Dr. Katja Trachte
Dr. Rütger Rollenbeck
Dr. Dietrich Göttlicher
Laboratory for Climatology and Remote Sensing,
University of Marburg, Deutschhausstr. 10, 35032
Marburg, Germany
bendix@staff.uni-marburg.de

Enrique Palacios
Instituto Nacional de Meteorología e Hidrología del
Ecuador, Iñaquito N36-14 y Corea, Quito, Ecuador
epalacios@gmx.net

Prof. Dr. Thomas Nauß
Faculty of Geography, University of Marburg,
Deutschhausstr. 10, 35032 Marburg, Germany
nauss@staff.uni-marburg.de